

Accepted for publication in the *Astronomical Journal*

The BTC40 Survey for Quasars at $4.8 < z < 6$ ¹

Eric M. Monier^{2,3,4}, Julia D. Kennefick^{4,5}, Patrick B. Hall^{4,6}, Patrick S. Osmer³,
Malcolm G. Smith⁷, Gavin B. Dalton⁵, & Richard F. Green^{4,8}

ABSTRACT

The BTC40 Survey for high-redshift quasars is a multicolor search using images obtained with the Big Throughput Camera (BTC) on the CTIO 4-m telescope in V , I , and z filters to search for quasars at redshifts of $4.8 < z < 6$. The survey covers 40 deg^2 in B , V , & I and 36 deg^2 in z . Limiting magnitudes (3σ) reach to $V = 24.6$, $I = 22.9$ and $z = 22.9$. We used the $(V - I)$ vs. $(I - z)$ two-color diagram to select high-redshift quasar candidates from the objects classified as point sources in the imaging data. Follow-up spectroscopy with the AAT and CTIO 4-m telescopes of candidates having $I \leq 21.5$ has yielded two quasars with redshifts of $z = 4.6$ and $z = 4.8$ as well as four emission line galaxies with $z \approx 0.6$. Fainter candidates have been identified down to $I = 22$ for future spectroscopy on 8-m class telescopes.

Subject headings: surveys — quasars: general

¹Based on observations performed at the Blanco 4-m telescope at the Cerro Tololo Inter-American Observatory and the Anglo-Australian Telescope

²monier@astronomy.ohio-state.edu

³Department of Astronomy, The Ohio State University, 140 W. 18th Ave., Columbus, OH 43210

⁴Visiting Astronomer, CTIO, National Optical Astronomy Observatories, which is operated by the Association of Universities for Research in Astronomy, Inc. (AURA) under cooperative agreement with the National Science Foundation.

⁵NAPL, Keble Road, Oxford OX1 3RH, England, UK

⁶Princeton University Observatory, Princeton, NJ 08544-1001, and Pontificia Universidad Católica de Chile, Departamento de Astronomía y Astrofísica, Facultad de Física, Casilla 306, Santiago 22, Chile

⁷Cerro Tololo Inter-American Observatory, Casilla 603, La Serena, Chile

⁸National Optical Astronomy Observatories, P.O. Box 26732, Tucson, AZ 857726

1. Introduction

Surveys for faint quasars at $z > 4.5$ and the subsequent constraints they place on the quasar luminosity function (QLF) will eventually determine how luminosity evolution and density evolution each contribute to the declining space density of quasars established for $3 \lesssim z \lesssim 4.3$ (Warren, Hewett, & Osmer 1994, hereafter WHO; Schmidt, Schneider, & Gunn 1995, hereafter SSG; Kennefick, Djorgovski, & DeCarvalho 1995) and now observed out to redshifts of $z \sim 5$ (Fan *et al.* 2001b). The QLF in turn is an important input to models of structure formation in the early Universe (Haehnelt, Natarajan & Rees 1998).

Additionally, high-redshift quasars provide insight into the nature of quasars and their environments in the early Universe (Haehnelt & Kauffmann 2000), contribute to the ionizing UV background (Madau, Haardt & Rees 1999), and act as background illumination for absorption-line studies of the intergalactic medium. It is therefore important to continue to search for quasars of all luminosities at the highest possible redshifts, and thus the earliest possible epochs.

We began this survey to address the shape of the QLF at redshifts $z \gtrsim 5$. WHO found evidence that the positive evolution in the QLF at $0 < z < 2.2$ continues to $z \approx 3.3$ and then the space density declines by a factor of 6.5 at $z = 4$. SSG found that space densities have a maximum between $z = 1.7$ and 2.7 and then decrease by a factor of 2.7 per unit redshift beyond $z = 2.7$. Extrapolations of these QLF's to $5 < z < 6$ predict 0.02 (WHO) to 0.6 (SSG) quasars per deg^2 to $I = 22$.

The major effort to find quasars at higher redshifts is the Sloan Digital Sky Survey (SDSS), which continues to be remarkably successful at finding $z > 4$ quasars. SDSS has discovered more than 100 such objects including one at $z = 6.3$, the most distant published (see, e.g. Fan *et al.* 2000, 2001c; Anderson *et al.* 2001). However, SDSS is limited to $z > 4.5$ quasars with $M_B \lesssim -26$ and misses the bulk of the population, which is found at lower luminosities. Thus, there is a need for surveys to find less luminous $z > 4.5$ quasars to address the shape of the faint end of the QLF. Sharp *et al.* (2001) have presented initial results from one such survey, finding two $z > 4.5$ quasars to $i \approx 21.5$ in 10 deg^2 of *griz* data.

The BTC40 survey is a deep, 40 deg^2 survey in *BVIz* filters undertaken to search for clusters of galaxies, morphologically-selected gravitational lenses, and quasars at $z \gtrsim 4.8$. The results on clusters and gravitational lenses will be presented elsewhere. In this paper we present results of our efforts using a 4-m telescope and large format camera to complement the SDSS quasar search and extend it to lower luminosities.

We used the *VIz* imaging data to select quasar candidates over 36 deg^2 of sky down to $I \leq 22$, corresponding to absolute magnitudes of $M_B \lesssim -24.7$ at $z = 4.8$. The selection

process compared the expected colors of quasars at redshifts $4.8 < z < 6$ to the locations of catalogued stellar objects in $(V - I)$ vs. $(I - z)$ color space. Follow-up spectroscopy at the CTIO 4-m and AAT was attempted to $I < 21.5$ and has resulted in the discovery of two quasars with redshifts of $z = 4.6$ and $z = 4.8$, as well as several emission-line galaxies at $z \approx 0.6$. Spectroscopy of the fainter candidates, down to $I = 22$, will be the focus of our future efforts on larger telescopes.

We describe the survey imaging data in §2, the candidate selection in §3, and the follow-up spectroscopy in §4. We discuss our results in §5.

2. Imaging

2.1. Observations

The Big Throughput Camera (Tyson *et al.* 1992; Wittman *et al.* 1998) contains a 2×2 array of thinned 2048×2048 SITE CCDs with $24\mu\text{m}$ pixels. Used at the prime focus of the CTIO 4-m Blanco Telescope (and since replaced by the MOSAIC camera), the BTC plate scale is $0''.43 \text{ pixel}^{-1}$, resulting in a sky area of $14'7 \times 14'7$ imaged by each CCD. The CCDs are separated by $5'4$, for non-contiguous coverage of 0.24 deg^2 per pointing.

Six survey fields (Table 1) were selected with declinations to provide low airmass, and $|b|$ chosen to minimize Galactic H I and contamination by stars. The survey was split between spring and fall data sets, each containing three fields separated by ~ 2.5 hours in right ascension.

Initial BTC imaging in the Johnson-Cousins BV and Kron-Cousins I filters was performed at the Blanco 4-m telescope at CTIO in the spring and fall semesters of 1997 (Table 2). A “lawn-mowing” pattern was used, in which the telescope moved back and forth first in right ascension and then in declination. An overlap of $1'$ in both directions provided continuity between adjacent pointings for later “bootstrapping” of the photometry.

The V and I data were reduced and catalogs produced (both procedures are described below for the full data set) and ≈ 200 objects with $(V - I) > 4.0$ were selected as candidates for $z > 5$ quasars. The B data were not used for the quasar survey because the $B - V$ color provides no useful information for finding high-redshift quasars; the 912 \AA Lyman limit is well into the B filter by $z = 4.8$, while the flux in V is heavily depressed by the Ly α forest. Spectroscopy was performed at the CTIO 4m on 20 of the brighter candidates under poor conditions in 1998 April. All of these candidates turned out to be late-type (M5 or later) stars. In light of this result, we resolved to improve the survey efficiency and reduce cool-

star contamination of the quasar candidate sample by obtaining follow-up imaging in the near-infrared z filter.

The z filter in use at CTIO is a longpass filter matching the response of the z' filter in the SDSS (Fukugita *et al.* 1996; Gunn *et al.* 2001). The filter uses RG830 Schott color glass to provide the short-wavelength cutoff, and the long-wavelength response is determined entirely by the decreasing sensitivity of the CCD past 9000 Å. The combined CCD and filter response curves are shown in Figure 1. By extending coverage into the near-IR past I , the z filter provides a means of distinguishing quasars from late-type stars. At redshifts of $z \approx 5$, the quasar Ly α $\lambda 1216$ emission line moves into the I filter at ≈ 7250 Å. Quasars thus become progressively bluer in $(I - z)$ than late-type stars of similar $(V - I)$ (see §3), allowing for the separation of the quasars from the stars in color-color space. Imaging of the survey fields in the z -band was performed in 1998 November and 1999 February (Table 2). ⁹

2.2. Data Reduction

We processed the imaging data by using the CCDRED task in the IRAF¹⁰ software package to correct the object and calibration frames from each observing run for overscan and bias. For each CCD chip, we median-combined and normalized the dome flats from each night and used them to remove pixel-to-pixel variations in the field and standard-star frames. We then took all of the field images from the run and median-combined them to create “super sky” flats for the four CCD chips. After smoothing these flats we used them as illumination corrections to remove the large-scale variations across each chip. Finally, to correct for fringing in the I and z data, we took the unsmoothed super-sky flats, scaled them with the *defringe*¹¹ task to the level of the individual object frames, and subtracted them from those frames.

⁹CCDs 1 and 2 of the BTC were replaced in 1998 May, between the BVI and the z runs.

¹⁰IRAF is distributed by the National Optical Astronomy Observatories, which are operated by the Association of Universities for Research in Astronomy, Inc., under cooperative agreement with the National Science Foundation.

¹¹Part of Pat Hall’s Add-on Tasks (PHAT) under IRAF.

2.3. Catalogs

We processed the reduced images with the SKICAT software package (Weir *et al.* 1995) to generate our object catalogs. Briefly, SKICAT uses FOCAS (Jarvis & Tyson 1981; Valdes 1982) for object detection, photometry, and object classification. The resulting catalogs reside in an online SYBASE database and are easily accessed through the SKICAT interface. Queries can be performed on the database to, e.g., select point sources within a given magnitude range. Our database contains approximately 476,000 stellar objects with $I \geq 16$ down to the 3σ limits ($V = 24.6$, $I = 22.9$, $z = 22.9$) of the survey.

An important component of SKICAT is the ability to match features between catalogs based on their measured positions. For this survey, our objective was to construct matched VIz catalogs of objects classified as point sources in the I filter and use them to create $(V - I)$ vs. $(I - z)$ two-color diagrams of the survey area, as described in §3. Construction of the matched catalogs relies on the object coordinates, therefore the astrometry of the objects must be accurate.

2.4. Astrometry

The large field of view of the BTC results in images with significant geometric distortions due to sky curvature, slight rotations between the chips and distortions of the prime focus corrector (Wittman *et al.* 1998). Therefore, accurate astrometry of objects catalogued in this survey had to be established before matching could be performed between filters. We used the *undist* ray tracing program (written by I. Dell'Antonio) in a two-step process to correct the positions contained in the object catalogs. For a given pointing (including RA, Dec, hour angle and filter) the program generates a grid of CCD x,y pairs with corresponding RA and Dec, based on the known optical properties of the BTC and several input parameters (field center, hour angle, filter, and date of observing run). The IRAF tasks *geomap* and *geoxytran* use the output spatial information to compute and perform the transformation from the FOCAS x,y coordinates of cataloged objects into RA and Dec values.

A first run through this process produced an initial correction to the object coordinates. We then downloaded USNO catalogs (Monet *et al.* 1998) of the stars in the areas of the sky covered by each pointing and compared the coordinates of stars common to the USNO and survey catalogs to produce a set of offsets ranging from a few arcseconds up to $\sim 2'$ for some fields. We used these as the input to a second pass of the IRAF routines to refine the transformation, and from this result calculated new object coordinates and updated the database. The RMS residuals on the fit to the USNO coordinates were on the order of ≈ 0.4

arcseconds.

2.5. Photometry

Conditions during the imaging runs were generally not photometric. To calibrate the data we determined initial rough zero points for the data from standard stars observed at the beginning and end of each night. In an initial test of the candidate selection criteria (§3), the position of the stellar locus in color-color space fluctuated from field to field, indicating changing conditions over the course of the run and the individual nights. Portions of some nights may have been photometric, but standard-star observations obtained under photometric conditions were not extensive enough to allow a precise photometric solution for the full data set. However, note that when selecting high-redshift quasar candidates only accurate differential photometry is crucial. Candidates are chosen by where they lie with respect to the stellar locus in color-color space, making absolute photometry less critical.

Nevertheless, we took several steps to ensure the accuracy of the absolute photometry. We created a model stellar locus using the Bruzual-Persson-Gunn-Stryker (BPGS) spectrophotometric atlas available in the STSDAS/SYNPHOT package under IRAF. This atlas is an extension of the Gunn-Stryker optical atlas (Gunn & Stryker 1983) into the UV and also includes infrared data from Strecker, Erickson, & Whittenborn (1979). The stellar locus results from folding the colors through the combined CCD/filter response and plotting the resulting $(V - I)$ vs. $(I - z)$ colors. After creating and examining color-color plots of $(V - I)$ vs. $(I - z)$ for individual pointings, we selected a pointing from the spring dataset as having been taken under near-optimal conditions based on the tightness of the observed stellar locus and its overlap of the model stellar locus. We determined the shifts in color-color space needed to put each pointing onto the same scale by using a light table and evaluating the necessary shifts by eye. We eliminated four pointings of Field 6 from candidate selection based on the low numbers of objects and the degree of scatter in the resulting stellar locus. Visual inspection of these fields and the observing logs indicate conditions were especially poor at the time of these observations.

One of the survey fields was originally chosen to overlap part of the faint photometric calibration sequence of Boyle *et al.* (1995). We compared our final photometry of the sources in this 6×6 arcminute overlap region to the values from the catalogs of Field 866 in Boyle *et al.*. The result is shown in Figure 2. The magnitudes agree well for $I < 19$, neglecting the two brightest objects, which are saturated in the BTC40 data. At the fainter end, however, the figure suggests a discrepancy of several tenths of a magnitude between the two measurements. We intend future observations of the survey fields to refine the survey

photometry, but, as noted above, the relative photometry was adequate for selecting high-redshift quasar candidates.

The journal of observations in Table 2 includes the average 3- and 5- σ magnitude limits reached in each survey field. The average limiting magnitudes (5 σ) for the imaging data over the entire survey are $V = 24.0$, $I = 22.4$, and $z = 22.4$ (AB₉₅). Note that the original BTC CCD chip #1 was less sensitive than the other three, especially in the blue (Wittman et al 1998). As a result, the 5 σ limiting magnitudes for chip #1 in V are $\Delta m_{lim,V} \approx 0.1 - 0.3$ brighter than those of chips #2, #3, & #4. The chip #1 sensitivity in the I filter was less discrepant, keeping any effect on the limiting magnitude $\Delta m_{lim,I} \leq 0.1$ for chip #1 I data. Because the V data are much deeper than the I data, and candidate selection was limited to $I \leq 21.5$ variations in chip sensitivity ultimately did not influence candidate selection.

3. Candidate Selection

The general region of $(V - I)$ vs. $(I - z)$ color space in which $4 < z < 6$ quasars will be found is readily seen in Figure 3, a plot of the stellar sequence taken from the BPGS stellar atlas in the STSDAS/SYNPHOT package. The quasar colors are from synthetic quasar spectra as described in Kennefick *et al.* (1996). We used this predicted region as a guide to selecting initial candidates from $(V - I)$ vs. $(I - z)$ diagrams of BTC40 objects classified as point sources (FOCAS 'stars' or 'fuzzy stars') in the I -band data. We performed a visual inspection of the images of those candidates to ensure the colors had not been skewed by cosmic ray hits or cosmetic flaws in the CCDs. Finally, a priority was assigned to each candidate based on the magnitude, location in color-color space, and the visual inspection.

The selection process for our initial spectroscopy runs used magnitudes as calculated in SKICAT using FOCAS as described by Weir *et al.* (1995). FOCAS calculates two magnitudes: an aperture magnitude calculated within a specified radius (we used three pixels during SKICAT processing), and a 'total' magnitude based on an area of twice the detection area. As discussed by Weir *et al.* (1995), the total magnitude carries the associated risk of increased random error. After our first observing run in 1999 November at CTIO, in which only one observed candidate turned out to be a quasar, we compared the FOCAS photometry to magnitudes measured independently with PHOT in IRAF. We concluded that for faint point sources the random errors in the SKICAT/FOCAS measurement can be significant, moving stars out of the stellar locus and into the region of quasar candidate selection (and presumably vice versa).

Therefore, we re-measured the magnitudes using the IRAF PHOT package and an

aperture radius of two pixels (roughly twice the seeing) and proceeded to compile candidate lists based on the colors resulting from the IRAF photometry. Objects that were also in the selection area using FOCAS colors were given higher priority for follow-up spectroscopy. The initial spectroscopy runs allowed us to refine the selection criteria and estimate how close to the stellar locus we could reasonably hope to go. This determination requires balancing the number of candidates selected with the increasing likelihood of contamination by the cool stellar population as one moves closer to the stellar locus. Figure 4 shows the stellar locus from a portion of the survey data overplotted with the complete candidate set broken down by magnitude range. The objects in the region below and to the right of the lines satisfy the criteria used in selecting candidates.

4. Spectroscopy

We performed follow-up spectroscopy of selected candidates during three observing runs at the CTIO 4m and three at the AAT (Table 3). Over the course of these six runs we were able to observe 82 quasar candidates. However, many of these are not included in our later survey sample of sixty-two candidates with $I \leq 21.5$, due to (1) the adoption of IRAF photometry after the first observing run and (2) modifications to the selection criteria based on results of the initial runs. We observed 40 objects from the list of 62 candidates, 27 at CTIO and 13 at the AAT; several promising candidates with inconclusive initial spectra were observed at both telescopes. In this section we describe the setup at the two locations and the data reduction process.

4.1. CTIO

We used the RC Spectrograph at the CTIO 4m with similar setups on 1999 November 14-16, 2000 May 9-11, and 2000 October 16-17. The RC Spectrograph on the CTIO 4m uses the Blue Air Schmidt (BAS) camera and a Loral 3K CCD, which we formatted to 3071×800 for faster readout. We chose the G181 grating (316 lines/mm) and the GG495 blocking filter for a resolution of 2\AA pixel^{-1} over the range $\approx 5000 - 11000 \text{\AA}$. During good seeing conditions we maintained the slit width at $1''$ and opened it to $1''.5$ when the seeing deteriorated. Exposure times ranged from 900s to 3600s, depending on the brightness of the candidate. We observed 27 candidates from our sample over the course of the three runs, down to a cutoff magnitude of $I \simeq 21.5$.

4.2. AAT

We performed the spectroscopy at the AAT using LDSS++ with the 165 Å/mm grating for a dispersion of 2.6Å pixel, providing coverage over \sim 5200-10000Å. We used a longslit 1" wide when possible, but in general we were limited by unfavorable conditions to a slit width of 1".7. LDSS++ can be operated in “nod and shuffle” mode (Glazebrook & Bland-Hawthorn 2001), in which the telescope is nodded rapidly by 10–20" while the spectra are recorded on two adjacent regions of the MIT Lincoln Lab (MITLL) CCD through charge shuffling. The method allows optimal sky subtraction and is ideal for extracting fainter targets. Conditions were fair to poor for most of three observing runs, and we observed 13 candidates from our survey list.

4.3. Data Reduction

We reduced the candidate spectra with CCDRED under IRAF, including subtracting the overscan region and flatfielding the data using quartz flats obtained during the runs. For the nod-and-shuffle AAT data we performed the additional step of subtracting the two exposed regions of the CCD, effectively eliminating the night sky emission lines. We used the IRAF ‘apall’ task to select and size the apertures interactively and trace the spectra across the chip. We also specified the regions used for background subtraction in the CTIO data. We extracted arc calibration spectra by using traces obtained from standard-star spectra, used the ‘identify’ task on the arc spectra to obtain a dispersion solution, and proceeded to apply this solution to the extracted spectra of the candidates. Finally, we combined spectra of objects having multiple exposures. We also used extracted standard-star spectra to get the shape of the object spectra and a rough flux calibration.

4.4. Spectroscopic Results

The positions, I magnitudes, colors, and, where possible, identifications of the observed candidates are given in Table 4. The list includes two quasars, ten stars, three compact narrow emission-line galaxies (CNELGs), 15 objects that could not be identified due to the low S/N of the spectra, and 9 objects with spectra too faint to be extracted (but possessing no obvious emission lines).

4.4.1. Quasars

Two of the identified objects are quasars at redshifts $z \simeq 4.6$ and $z \simeq 4.8$ and magnitudes of $I = 19.4$, toward the brighter limit of our survey. Finding charts for these quasars are given in Figure 5, and the spectra are presented in Figure 6. Both quasars show strong Ly α /N V emission and weaker emission due to C IV. Continuum flux shortward of Ly α is depressed by the intervening Ly α forest.

One of the quasars, BTC40 J2340–3949, was detected in the deep, 1.4GHz ATESP radio survey (Prandoni *et al.* 2000) with a peak flux of 0.57 mJy. We can adapt the radio-optical flux ratio, R_{r-o} , of Kellerman *et al.* (1989) for a high-redshift source, substituting the I -band (8000 Å) magnitude for the B -band (4400 Å) and scaling the radio flux to the proportionally lower frequency $\nu(8000/4400)^{-1}$ by assuming a power law of the form $f \sim \nu^{-0.5}$. In this case, $R_{r-o} \approx 10$, putting the quasar just on the border of being classified as radio-loud. BTC40 J2340–3949 may have a weak BAL trough (or strong associated absorption) seen in N V at ≈ 6945 Å and C IV at ≈ 8680 Å (the absorption at 7600 Å is atmospheric), and may therefore be similar to the radio-moderate BAL quasars discovered in large numbers by the FIRST Bright Quasar Survey (Becker *et al.* 2000).

4.4.2. Compact Narrow Emission Line Galaxies

We report the discovery of three compact narrow emission line galaxies (CNELGs) with $0.55 < z < 0.6$. The positions, I magnitudes and colors are provided for the CNELGs, in Table 4, finding charts are given in Figure 7, and the spectra are shown in Figure 8. The galaxies exhibit point-source profiles and [O III] $\lambda\lambda 4959, 5007$ emission (Figure 8) shifted into the I filter at $z \approx 0.6$, giving them colors similar to our quasar candidates. All three galaxies have $(V - I) \approx 1.7$, making them, along with the quasar BTC40 1429+0119 ($V - I = 1.71$), the bluest ($V - I$) candidates in the sample (see Figure 4). Contamination by such galaxies has been encountered by other surveys for quasars at lower redshift (see, e.g. Hall *et al.* 1996 and Kennefick *et al.* 1997). In addition to [O III], the spectra show [O II] $\lambda 3727$ and probable [Ne III] $\lambda 3869$, as well as H β in one case.

BTC J0949+0715 is almost certainly a Seyfert 2 galaxy, based on the emission line diagnostics of Baldwin, Phillips, & Terlevich (1981) and Rola, Terlevich, & Terlevich (1997). Even though H β is detected in this object, it is very weak relative to [O III] $\lambda 5007$, and such a ratio is a good sign of AGN activity.

The other galaxies appear to be starburst galaxies, though within the fairly large uncertainties, BTC J1430+0107 could be an AGN as well.

Finally, we note the serendipitous discovery of a galaxy at $z = 0.58$, as measured from narrow O III, O II, and H β emission lines seen in the spectrum (Figure 8, bottom panel). The galaxy is too faint for its morphology to be established from the BTC image, but it lies 36" due north of quasar candidate BTC40 J2345-3948. Since the slit was oriented N-S, spectra for the candidate and galaxy were obtained simultaneously.

5. Discussion

In our high-redshift quasar survey we have found two $I < 21.5$ quasars with $z = 4.6$ and $z = 4.8$ in 36 deg^2 , proving the validity of the selection technique. Although our candidate selection is designed to be most sensitive for $z \gtrsim 4.8$, when the Ly α emission line has moved into the I filter, slightly lower-redshift “lyman-break” quasars may also enter the sample. This was the case with the BTC2340–3949.

To compare our results with SDSS, Anderson *et al.* (2001) found 29 quasars with $z \gtrsim 4.5$ in $\approx 700 \text{ deg}^2$ of the SDSS commissioning data, for a surface density of 1 quasar per 24 deg^2 to $i^* \leq 20.5$. Four of these quasars had $z > 5$, or 1 per 175 deg^2 . In the fall equatorial stripe of the SDSS commissioning data, Fan *et al.* (2001a) found 5 quasars with $4.5 \leq z \leq 4.77$ to $i^* \lesssim 20$ in 182 deg^2 , or 1 in 36 deg^2 . Thus, our findings from the BTC40 survey are consistent with the early SDSS results, although the BTC40 statistical base is admittedly very small.

More formally, the expected number of quasars predicted by a given survey may be computed by numerically integrating the QLF determined by the survey over the redshift and magnitude ranges of interest, and multiplying by the efficiency of the survey. Although we have not found enough quasars to derive a luminosity function, our results can be compared to predictions based on the QLF determined by the SDSS team.

Fan *et al.* (2001b) used the 39 quasars from the SDSS commissioning data to derive a QLF over the range $3.6 < z < 5$ and $-27.5 < M_{1450} < -25.5$, where M_{1450} is the absolute continuum magnitude measured at $\lambda = 1450(1+z)$ Å and calculated in the AB system. Since our quasar spectra are not spectrophotometric we scaled them to return the I magnitudes previously measured from the imaging data and then determined AB($1450(1+z)$). Assuming the continuum follows a power law with slope $\alpha = -0.5$, then $M_{1450} = -26.6$ for BTC40 J2340–3949 and $M_{1450} = -26.8$ for BTC40 J1429+0119, and both quasars occupy the parameter space probed by SDSS.

When integrated over $4.5 < z < 5$, the luminosity function of Fan *et al.* (2001b) predicts a surface density of ≈ 0.026 quasars per square degree down to $i' \approx 20.3$, or $I = 19.89$ using

the conversion between the AB and conventional magnitude systems from Fukugita *et al.* (1996). In the 36 deg² of the BTC40 survey, therefore, we would expect to find ≈ 1 quasar with redshift $4.5 < z < 5$ and $I < 19.9$, and in fact the two quasars we found fall into this category. Furthermore, the absence of $z > 5$ quasars in our sample to date is understandable, given their scarcity in the SDSS fields. The SDSS luminosity function predicts 0.015 quasars per deg² with $5 < z < 6$ to $I \approx 20$, or < 1 quasars in the 36 deg² of our survey.

The goal remains to determine the quasar luminosity function at fainter magnitudes. From the SDSS luminosity function over $4.5 < z < 5$ we would expect to find 10 quasars down to $I = 21.5$ and 20 quasars to $I = 22$ in our survey, while the QLF of SSG predicts 15 quasars to $I = 21.5$ and 35 to $I = 22$. Although we implemented candidate selection to $I = 21.5$, in the end we attempted spectroscopy of only five candidates with $I > 21$. None of the resulting spectra were good enough to allow identification, but most likely the objects are stars given the absence of any obvious emission lines. Constraining the number of faint quasars in our survey may require additional z -band imaging data to reduce the scatter in the color-color diagram at faint magnitudes and enable candidate selection closer to the stellar locus.

Follow-up spectroscopy on the $I > 21$ candidates will also necessitate the use of 8-10m telescopes to achieve a reasonable efficiency. In addition to the selected candidates down to $I = 21.5$ remaining to be observed, we have identified 275 potential candidates with $21.5 < I < 22$. Of course, effective use of time on the largest telescopes will require additional work to keep cool stars from ending up in the candidate list. As an example, Fan *et al.* (2001c) used J -band photometry to pare L- and T-type dwarfs from their list of i -band dropouts in a search for quasars at $z \simeq 6$.

In summary, to date we have obtained spectroscopic observations of the brightest candidates in our survey for high-redshift quasars. We have not yet found any quasars with $z > 5$, and in hindsight this is not surprising given the results from SDSS. But the SDSS results also predict our survey area will contain ~ 5 quasars with $z > 5$ to $I = 21.5$, and 11 to $I = 22$. The next important step is to follow up on the fainter objects, which will require observations with 8-m class telescopes.

6. Acknowledgements

We are grateful to G. Bernstein, T. Tyson and the BTC team for their years of effort devoted to the development and building of the BTC. We would like to thank Alberto Conti, Rick Pogge and Darren Depoy for their assistance with the z -band imaging. We also thank

the CTIO and AAO mountain staffs for their observing support. This work was supported by NSF grant AST-9802658.

REFERENCES

Anderson, S.F., Fan, X., Richard, G.T., Schneider, D.P., Strauss, M.A., Van den Berk, D.E., Gunn, J.E. 2001, AJ, 122, 503

Baldwin, J.A., Phillips, M.M., & Terlevich, R. 1981, PASP, 93, 5

Becker, R.H., White, R.L., Gregg, M.D., Brotherton, M.S., Laurent-Muehleisen, S.A., & Arav, N. 2000, ApJ, 538, 72

Boyle, B.J., Shanks, T., & Croom, S.M. 1995, MNRAS, 276, 33

Fan, X., *et al.* 2000, AJ, 120, 1167

Fan, X., *et al.* 2001a, AJ, 121, 31

Fan, X., *et al.* 2001b, AJ, 121, 54

Fan, X., *et al.* 2001c, AJ, 122, 2833

Fukugita, M., Ikchikawa, T., Gunn, J.E., Doi, M., Shimasaku, K., & Schneider, D.P. 1996, AJ, 111, 1748

Glazebrook, K., & Bland-Hawthorn, J. 2001, PASP, 780, 197

Gunn, J. E., & Stryker, L. L. 1983, ApJS, 52, 121

Gunn, J.E., *et al.* 1998, AJ, 116, 3040

Haehnelt, M.G., Natarajan, P., & Rees, M.J. 1998, MNRAS, 300, 817

Haehnelt, M.G., & Kauffmann, G. 2000, MNRAS, 318, L35

Hall, P.B., Osmer, P.S., Green, R.F., Porter, A.C., & Warren, S.J. 1996, AJ, 462, 614

Jarvis, J.F. & Tyson, J.A. 1981, AJ, 86, 426

Kellerman, K.I., Srakek, R., Schmidt, M., Shaffer, D.B., & Green, R. 1989, AJ, 98, 1195

Kennefick, J.D., Djorgovski, S.G., & de Carvalho 1995, AJ, 110, 2553

Kennefick, J.D., Djorgovski, S.G., & Meylan, G. 1996, AJ, 111, 1816

Kennefick, J.D., Osmer, P.S., Hall, P.B., & Green, R.F. 1997, AJ, 114, 2269

Madau, P., Haardt, F., & Rees, M.J. 1999, ApJ, 514, 648

Monet, D., Bird A., Canzian, B., Dahn, C., Guetter, H., Harris, H., Henden, A., Levine, S., Luginbuhl, C., Monet, A. K. B., Rhodes, A., Riepe, B., Sell, S., Stone, R., Vrba, F., &

Walker, R. 1998, The USNO-A2.0 Catalogue, (U.S. Naval Observatory, Washington DC).

Prandoni, I., Gregorini, L., Parma, P., de Ruiter, H.R., Vettolani, G., Wieringa, W.H., & Ekers, R.D. 2000, A&AS, 146, 41

Schmidt, M., Schneider, D. P., & Gunn, J. E. 1995, AJ, 110, 68 (SSG)

Sharp, R.G., McMahon, R.G., Irwin, M.J., & Hodgkin, S.T. 2001, MNRAS, 326, L45

Strecker, D. W., Erickson, E. F., & Whittenborn, F. C. 1979, ApJS, 41, 501

Rola, C.S., Terlevich, E., & Terlevich, R.J. 1997, MNRAS, 289, 419

Tyson, Bernstein, Blouke, & Lee 1992, SPIE 1656, 400

Valdes, F. 1982, *SPIE Proc. on Instrumentation in Astronomy IV*, 331, 465

Warren, S. J., Hewett, P. C., & Osmer, P. S. 1994, ApJ, 421, 412 (WHO)

Weir, N., Fayyad, U.M., Djorgovski, S.G., & Roden, J. 1995, PASP, 107, 1243

Wittman, D.M., Tyson, J.A., Bernstein, G.M., Lee, R.W., Dell’Antonio, I.P., Fischer, P., Smith, D.R., & Blouke, M.M. 1998, SPIE, 3355, 626

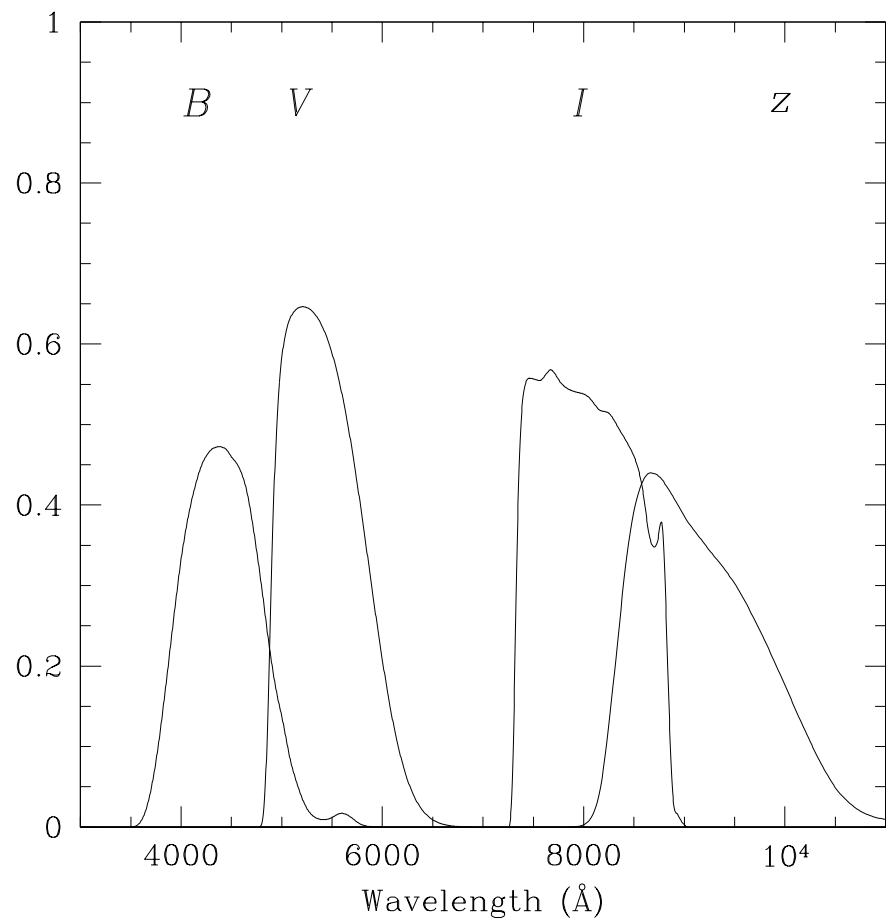


Fig. 1.— Response curves of the four filters used in the BTC40 survey, incorporating the filter response and CCD response.

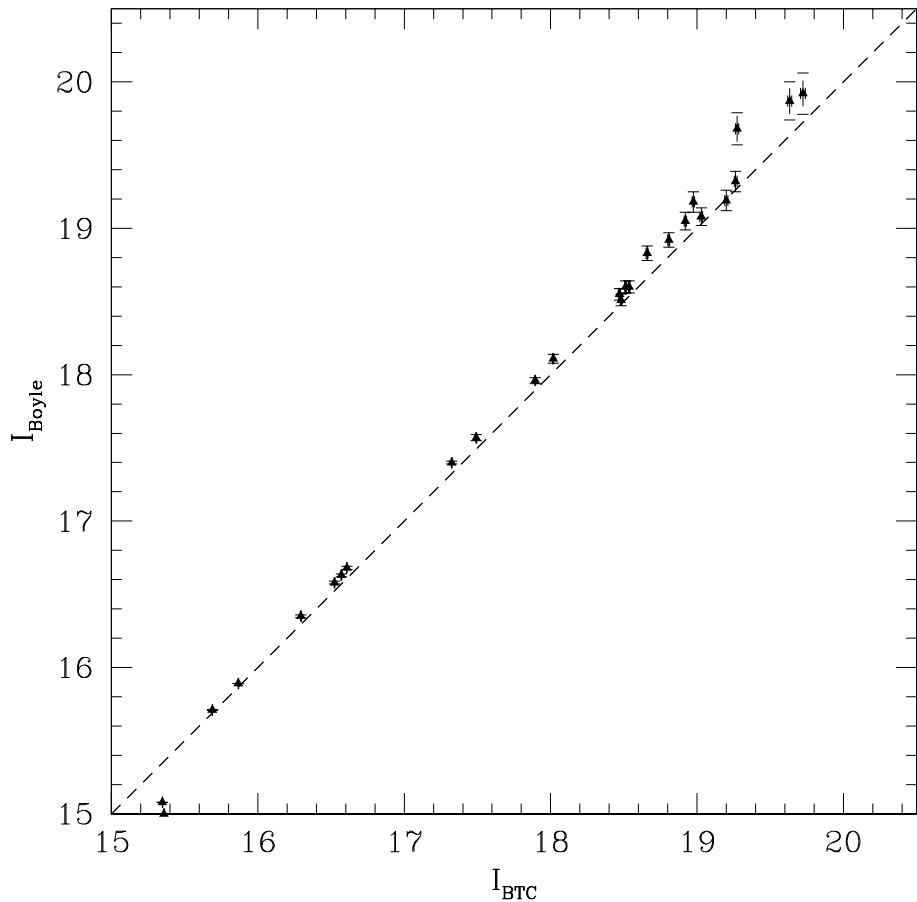


Fig. 2.— Comparison of the I magnitudes of stellar objects common to the BTC40 survey and Field 866 of Boyle *et al.* (1995). The two brightest objects in the lower left-hand corner are saturated in the BTC40 data.

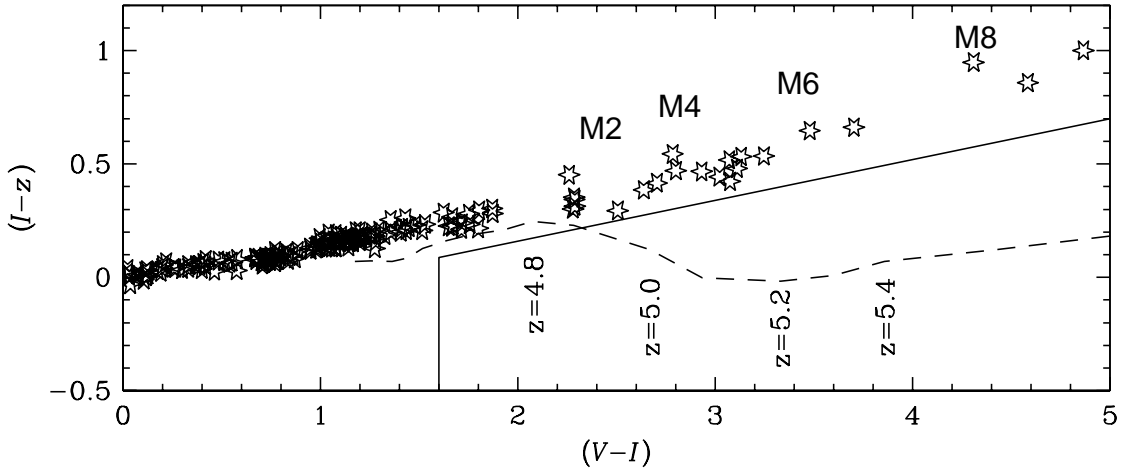


Fig. 3.— Plot of $(V - I)$ vs. $(I - z)$ colors showing the expected location of high-redshift quasars in color-color space, below and to the right of the solid selection lines. The dashed track follows the expected colors of quasars at redshifts from 4 to 6, with the colors of several redshifts marked. These colors were computed from 10 synthetic quasar spectra of varying continuum slopes and realizations of the Ly α forest in 0.1 redshift bins. At quasar redshifts of $z \sim 5$, quasars become progressively bluer in $(I - z)$ than the late-type stars of similar $(V - I)$, which enables the separation of the quasars from the stars in color-color space. The model stellar locus was calculated from the Bruzual-Persson-Gunn-Stryker spectrophotometric stellar database.

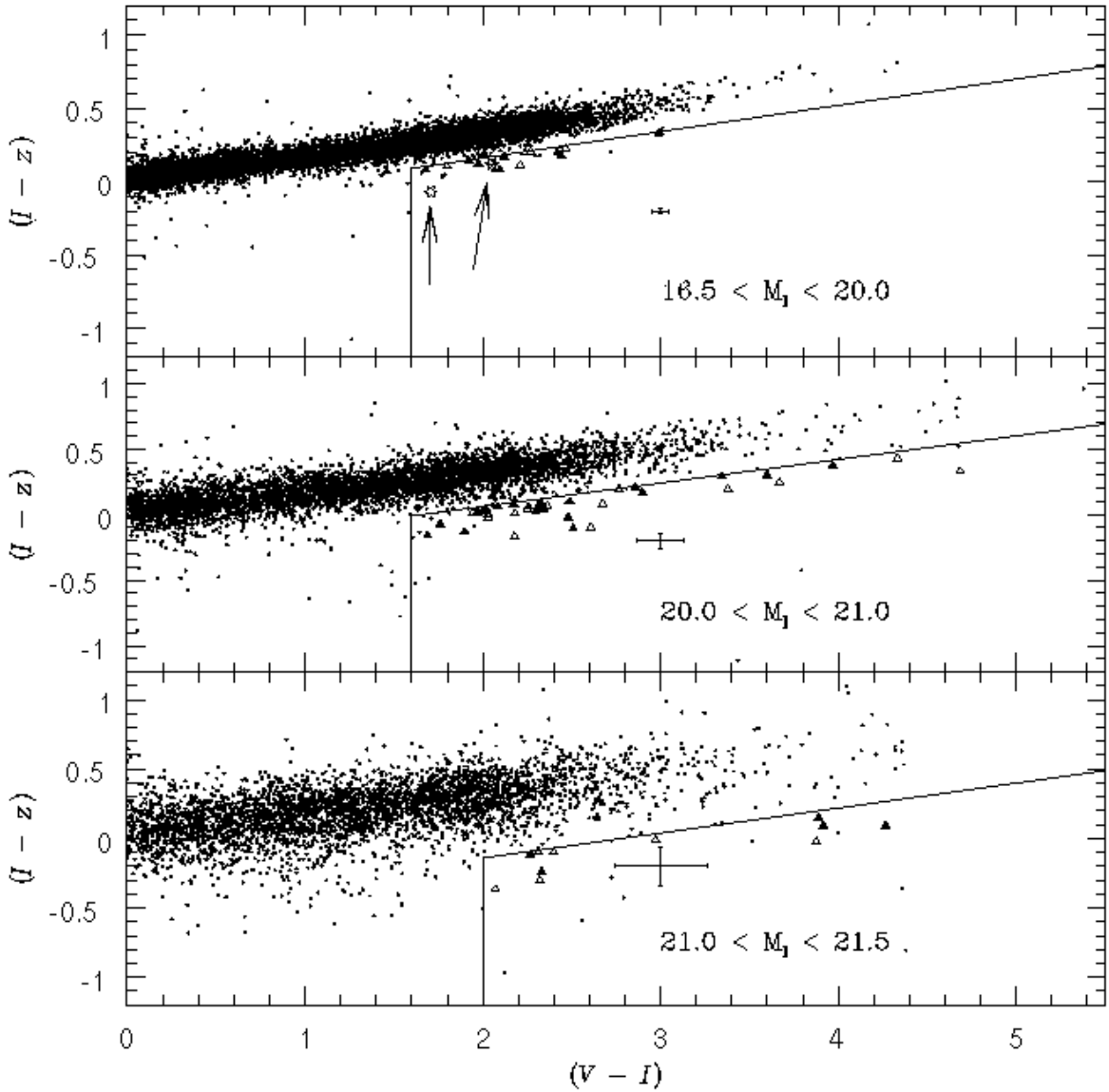


Fig. 4.— $(V-I)$ vs $(I-z)$ plots of stellar objects in 4.75 deg^2 (Field 3) of the survey overplotted with triangles to indicate the objects selected as high-redshift quasar candidates. Filled triangles represent candidates we observed spectroscopically. The two quasars discovered are the open stars indicated by arrows in the top panel. The CNELGs are the three filled triangles with $(V-I) \approx 1.7$ in the top and middle panels. Typical errors on the photometry are plotted for $(I-z) = -0.2$ and $(V-I) = 3.0$. Dots appearing in the selection areas are due to bad CCD columns or cosmic rays and were eliminated by visual inspection of the VIZ images during the candidate selection process.

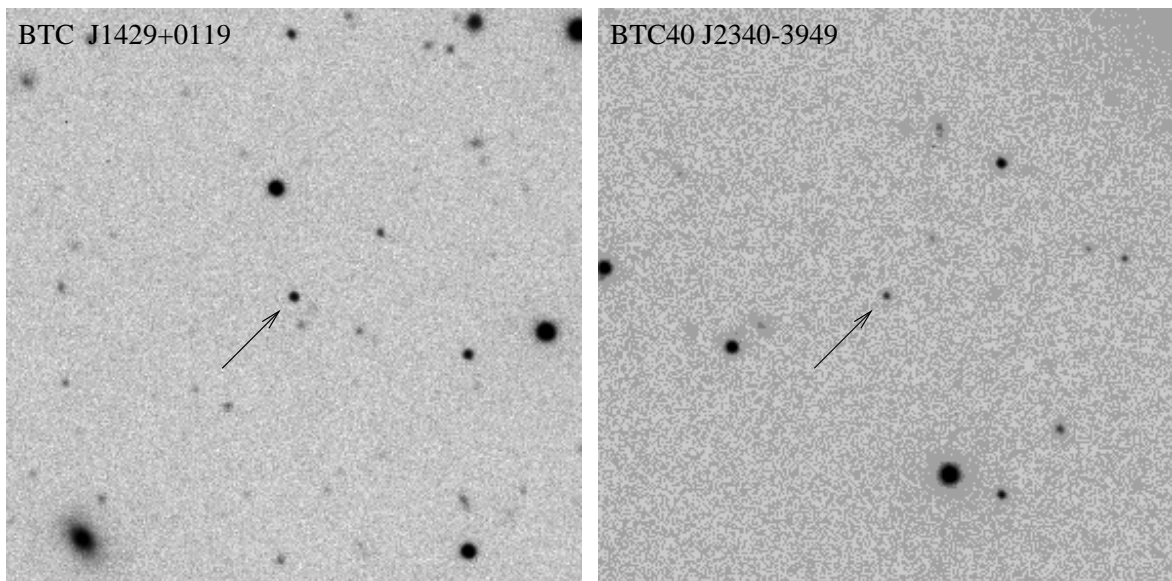


Fig. 5.— Finding charts for the two BTC40 quasars. The quasars are marked by arrows at the center, and the fields are 2' square. North is up and east is to the left.

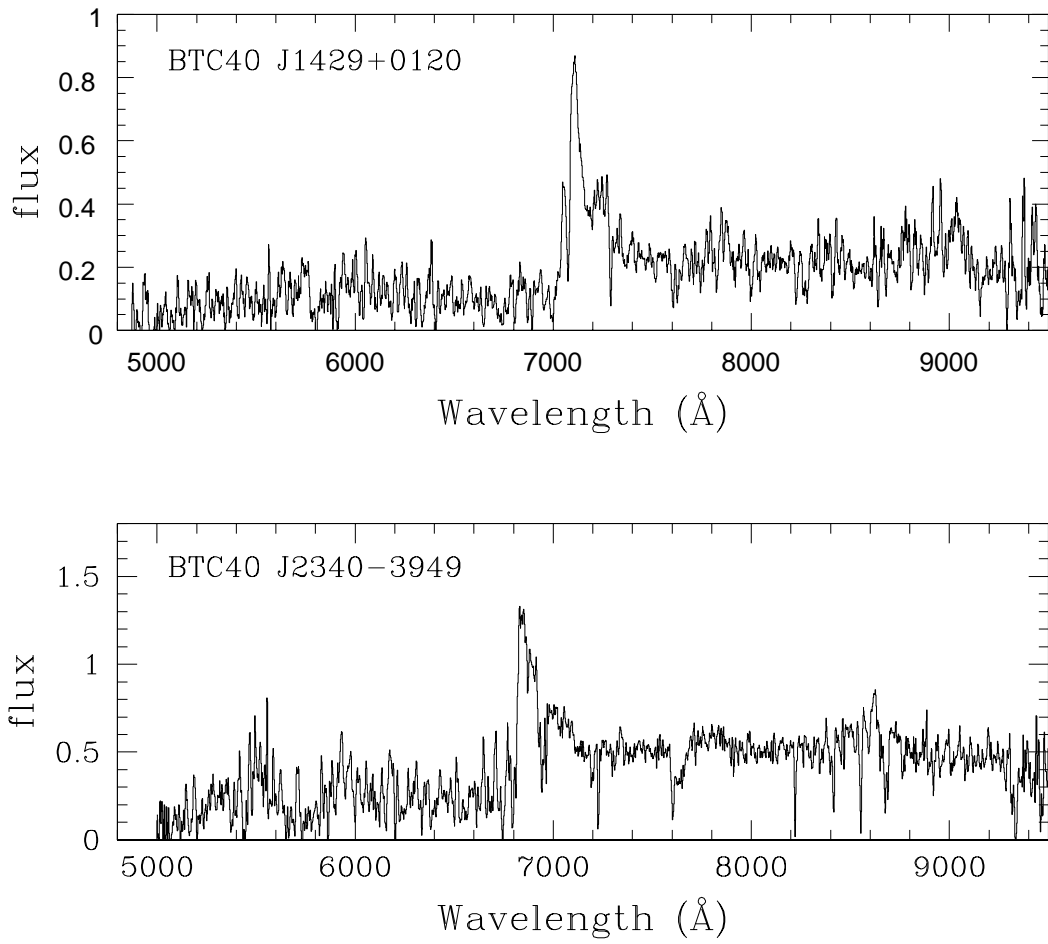


Fig. 6.— Spectra of the two quasars found in this survey, showing Ly α emission at $\sim 7000\text{Å}$ and continuum depression shortward of Ly α due to the Ly α forest. BTC40 J2340–3949 may have weak BAL troughs (or strong associated absorption) in N V at $\approx 6945\text{ Å}$ and C IV at $\approx 8680\text{ Å}$. The absorption at 7600 Å is atmospheric.

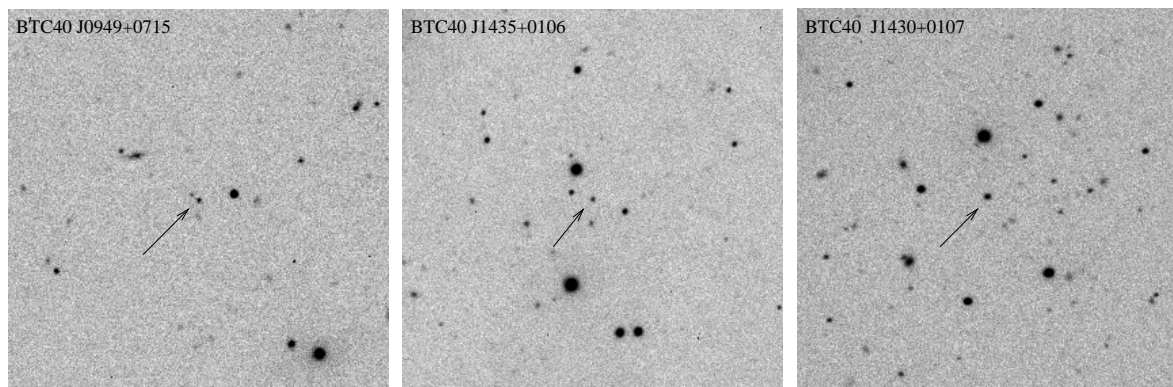


Fig. 7.— Finding charts for the three compact narrow emission line galaxies, marked by arrows in the center. The fields are 2' square. North is up and east is to the left.

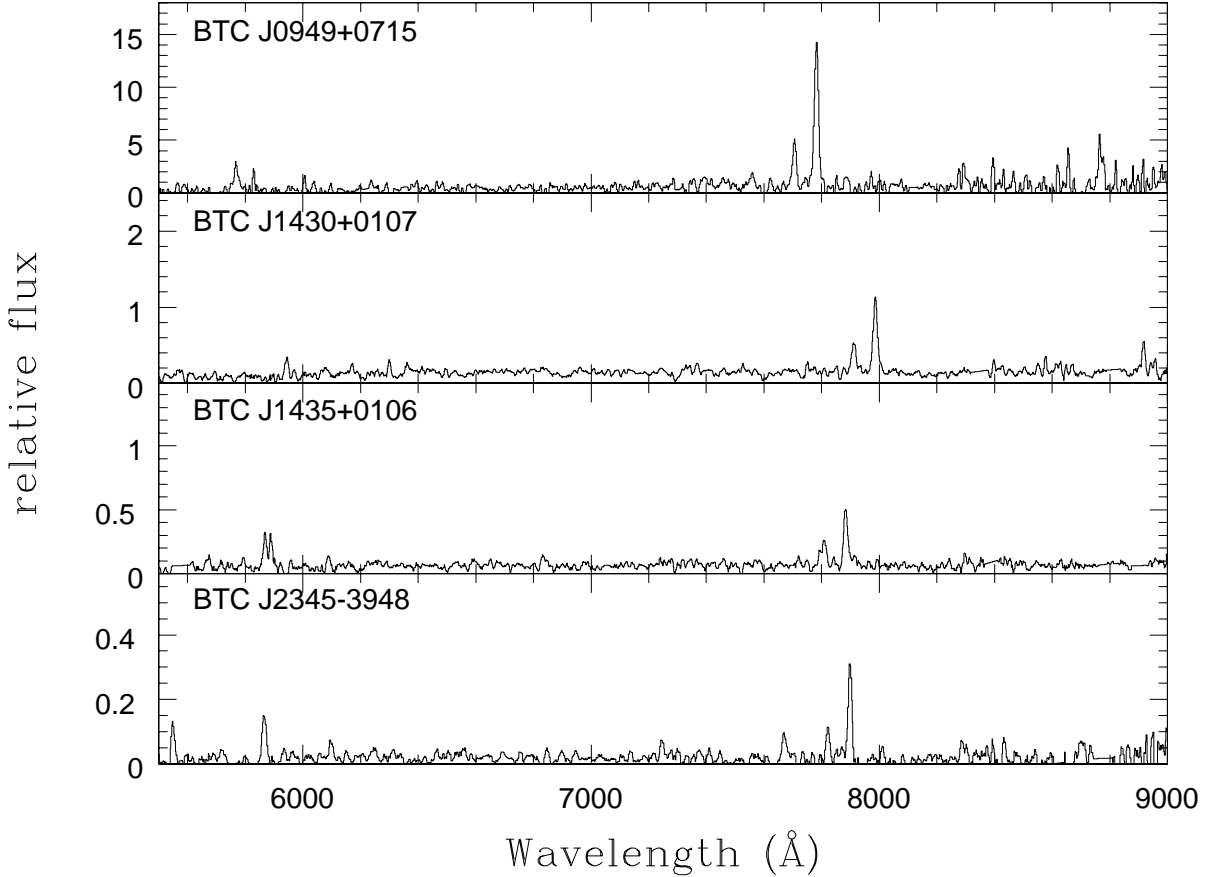


Fig. 8.— Spectra of four galaxies showing narrow emission lines due to [O III] $\lambda\lambda 4959, 5007$ and [O II] $\lambda 3727$ at $z \approx 0.6$. Weak H β $\lambda 4861$ can also be seen in the top and bottom objects; it may be present in BTC40 J1435+0106 but unfortunately lies atop an atmospheric absorption band where the noise is too large to allow its detection. The upper three galaxies are compact sources identified as quasar candidates prior to spectroscopy. The galaxy in the bottom panel was discovered serendipitously during spectroscopy of a nearby quasar candidate. The spectra are smoothed by five pixels and are interpolated across regions of poor sky subtraction.

Table 1. BTC40 Fields

Field	Field Center		l^{II}	b^{II}	Area ^a (deg ²)
	α (J2000)	δ (J2000)			
F1	09 50 41	07 06 51	229.4428	42.7567	5.76
F2	12 08 32	-19 44 16	289.2985	41.9954	7.68
F3	14 32 05	00 41 10	349.5323	54.1881	5.46
F4	23 52 14	-40 12 00	342.3103	-72.0884	3.84
F5	02 26 54	00 18 55	166.7328	-54.2300	5.76
F6	05 38 22	-28 12 44	232.3380	-27.4770	7.68

^aArea covered by the V , I , and z filters.

Table 2. Journal of CTIO Imaging Observations

Field	Filter	UT Date	Exp Time ^a (sec)	5 σ Limiting Magnitude	3 σ Limiting Magnitude
F1	<i>V</i>	14,16-17 Mar 1997	300	23.6 \pm 0.2	24.2 \pm 0.2
	<i>I</i>	14,16-17 Mar 1997	150	22.2 \pm 0.2	22.7 \pm 0.2
	<i>z</i>	21-22 Feb 1999	300	22.2 \pm 0.2	22.7 \pm 0.2
F2	<i>V</i>	14-17 Mar 1997	300	24.3 \pm 0.1	24.8 \pm 0.1
	<i>I</i>	14-17 Mar 1997	150	22.7 \pm 0.1	23.2 \pm 0.1
	<i>z</i>	21-22 Feb 1999	300	22.6 \pm 0.1	23.1 \pm 0.1
F3	<i>V</i>	14-17 Mar 1997	300	24.1 \pm 0.2	24.6 \pm 0.2
	<i>I</i>	14-17 Mar 1997	150	22.4 \pm 0.1	23.0 \pm 0.1
	<i>z</i>	21-22 Feb 1999	300	22.5 \pm 0.2	23.0 \pm 0.2
F4	<i>V</i>	26 Nov 1997	300	24.0 \pm 0.1	24.6 \pm 0.1
	<i>I</i>	26-27 Nov 1997	150	22.2 \pm 0.1	22.8 \pm 0.1
	<i>z</i>	24-25 Nov 1998	300	22.3 \pm 0.2	22.9 \pm 0.2
F5	<i>V</i>	24,26-27 Nov 1997	300	23.9 \pm 0.2	24.4 \pm 0.2
	<i>I</i>	24,26-27 Nov 1997	150	22.2 \pm 0.2	22.8 \pm 0.2
	<i>z</i>	25-27 Nov 1998	300	22.2 \pm 0.1	22.8 \pm 0.1
F6	<i>V</i>	24-27 Nov 1997	300	24.1 \pm 0.1	24.7 \pm 0.1
	<i>I</i>	24,26-27 Nov 1997	150	22.4 \pm 0.2	22.9 \pm 0.2
	<i>z</i>	24-25 Nov 1998	300	22.4 \pm 0.2	22.9 \pm 0.2

^aExposure time per pointing within a field.

Table 3. Journal of Spectroscopic Observations

Telescope	Instrument	UT Date
CTIO 4-m	R-C Spec	14-16 Nov 1999
AAT 4-m	LDSS	2-6 Dec 1999
AAT 4-m	LDSS	2-4 Apr 2000
CTIO 4-m	R-C Spec	9-11 May 2000
AAT 4-m	LDSS	29-31 Aug 2000
CTIO 4-m	R-C Spec	16-17 Oct 2000

Table 4. Results of QSO Candidate Spectroscopy

No.	Name	α (2000)	δ (2000)	I	$V - I$	$I - z$	Notes
1	BTC40 J0001-4025	00 01 20.6	-40 25 16	21.18	4.27	0.09	
2	BTC40 J0001-4023	00 01 34.3	-40 23 21	20.74	2.33	0.09	
3	BTC40 J0001-4025	00 01 50.5	-40 24 25	21.04	2.48	-0.02	
4	BTC40 J0002-4019	00 02 14.8	-40 19 52	20.78	1.97	0.02	
5	BTC40 J0223+0028	02 23 07.7	00 28 09	20.46	2.86	0.21	
6	BTC40 J0229+0023	02 29 58.7	00 23 05	20.32	2.18	0.11	
7	BTC40 J0233-0008	02 33 42.2	-00 08 20	20.48	2.05	0.14	
8	BTC40 J0528-2711	05 28 47.4	-27 11 30	19.80	1.90	-0.13	
9	BTC40 J0529-2854	05 29 56.1	-28 54 48	19.06	2.99	0.33	star
10	BTC40 J0537-2851	05 37 55.8	-28 51 01	20.11	2.51	-0.10	star
11	BTC40 J0544-2858	05 44 25.7	-28 58 28	18.63	1.46	0.07	star
12	BTC40 J0948+0637	09 48 43.9	06 37 55	20.17	3.97	0.37	
13	BTC40 J0949+0715	09 49 02.6	07 15 10	20.72	1.69	-0.16	ELG $z = 0.55$
14	BTC40 J0958+0733	09 58 59.5	07 33 57	20.04	2.01	0.19	star
15	BTC40 J1202-2014	12 02 44.6	-20 14 12	17.65	2.10	0.08	M star
16	BTC40 J1205-1918	12 05 02.9	-19 18 09	21.47	3.89	0.15	
17	BTC40 J1207-1916	12 07 47.7	-19 16 39	20.65	2.02	0.04	
18	BTC40 J1213-2022	12 13 14.8	-20 22 28	19.60	2.42	0.20	M star
19	BTC40 J1216-1913	12 16 18.3	-19 13 05	19.69	1.98	0.12	star
20	BTC40 J1216-1934	12 16 27.2	-19 34 48	20.73	2.30	0.03	
21	BTC40 J1423+0046	14 23 28.5	00 46 02	21.00	2.26	0.06	
22	BTC40 J1428+0119	14 28 49.8	01 19 33	20.77	2.34	0.05	
23	BTC40 J1429+0119	14 29 26.5	01 19 54	19.35	1.71	-0.08	QSO $z = 4.84$

Table 4—Continued

No.	Name	α (2000)	δ (2000)	I	$V - I$	$I - z$	Notes
24	BTC40 J1429+0108	14 29 45.7	01 08 55	20.91	2.18	0.07	
25	BTC40 J1429+0034	14 29 57.2	00 34 32	19.98	1.92	0.15	star
26	BTC40 J1430+0028	14 30 09.7	00 28 11	20.50	3.60	0.30	
27	BTC40 J1430+0107	14 30 10.9	01 07 22	19.88	1.68	0.08	ELG $z = 0.59$
28	BTC40 J1434+0033	14 34 36.3	00 33 13	20.93	2.32	0.09	
29	BTC40 J1435+0106	14 35 42.7	01 06 47	20.67	1.76	-0.07	ELG $z = 0.57$
30	BTC40 J1438+0043	14 38 24.8	00 43 23	20.61	3.35	0.29	
31	BTC40 J2340-3949	23 40 25.7	-39 49 32	19.40	2.05	0.12	QSO $z = 4.62$
32	BTC40 J2345-3948	23 45 27.5	-39 48 42	21.38	3.92	0.09	^a
33	BTC40 J2348-4018	23 48 55.4	-40 18 36	20.98	2.08	0.06	
34	BTC40 J2350-4020	23 50 06.6	-40 20 49	21.27	2.33	-0.24	
35	BTC40 J2354-4044	23 54 55.2	-40 44 19	20.33	2.00	0.03	
36	BTC40 J2356-3949	23 56 06.9	-39 49 57	19.62	2.44	0.18	star
37	BTC40 J2357-3944	23 57 10.1	-39 44 15	21.23	2.27	-0.12	
38	BTC40 J2358-3951	23 58 23.2	-39 51 04	19.60	2.12	0.17	star
39	BTC40 J2358-3950	23 58 31.3	-39 50 55	20.87	2.90	0.17	
40	BTC40 J2358-4022	23 58 52.3	-40 22 34	20.99	2.49	0.10	

^aAn emission-line galaxy at $z = 0.58$ lies 36" north of the candidate.